

Elucidating the Limit of Li Insertion into the Spinel $\text{Li}_4\text{Ti}_5\text{O}_{12}$

Haodong Liu, Zhuoying Zhu, Jason Huang, Xin He, Yan Chen, Rui Zhang, Ruoqian Lin, Yejing Li, Sicen Yu, Xing Xing, Qizhang Yan, Xiangguo Li, Matthew J. Frost, Ke An, Jun Feng, Robert Kostecky, Huolin Xin, Shyue Ping Ong, and Ping Liu

ACS Materials Lett., **Just Accepted Manuscript** • DOI: 10.1021/acsmaterialslett.9b00099 • Publication Date (Web): 24 May 2019

Downloaded from <http://pubs.acs.org> on May 25, 2019

Just Accepted

“Just Accepted” manuscripts have been peer-reviewed and accepted for publication. They are posted online prior to technical editing, formatting for publication and author proofing. The American Chemical Society provides “Just Accepted” as a service to the research community to expedite the dissemination of scientific material as soon as possible after acceptance. “Just Accepted” manuscripts appear in full in PDF format accompanied by an HTML abstract. “Just Accepted” manuscripts have been fully peer reviewed, but should not be considered the official version of record. They are citable by the Digital Object Identifier (DOI®). “Just Accepted” is an optional service offered to authors. Therefore, the “Just Accepted” Web site may not include all articles that will be published in the journal. After a manuscript is technically edited and formatted, it will be removed from the “Just Accepted” Web site and published as an ASAP article. Note that technical editing may introduce minor changes to the manuscript text and/or graphics which could affect content, and all legal disclaimers and ethical guidelines that apply to the journal pertain. ACS cannot be held responsible for errors or consequences arising from the use of information contained in these “Just Accepted” manuscripts.

Elucidating the Limit of Li Insertion into the Spinel



*Haodong Liu^{†=}, Zhuoying Zhu^{†=}, Jason Huang^{†=}, Xin He[‡], Yan Chen[§], Rui Zhang[‡],
Ruoqian Lin^{||}, Yejing Li[†], Sicen Yu[†], Xing Xing[†], Qizhang Yan[†], Xiangguo Li[†], Matthew J.
Frost[§], Ke An[§], Jun Feng[‡], Robert Kosteck[‡], Huolin Xin^{‡*}, Shyue Ping Ong^{†*}, Ping Liu^{†*}*

[†]Department of Nanoengineering, University of California San Diego, CA, 92093, USA

[‡]Energy Storage and Distributed Resources Division, Lawrence Berkeley National Laboratory, Berkeley, California 94720, USA

[§]Neutron Scattering Division, Oak Ridge National Laboratory, Oak Ridge, TN, 37830, USA

[‡]Department of Physics and Astronomy, University of California Irvine, CA, 92697, USA

^{||} Chemistry Division, Brookhaven National Laboratory, Upton, NY 11973, USA

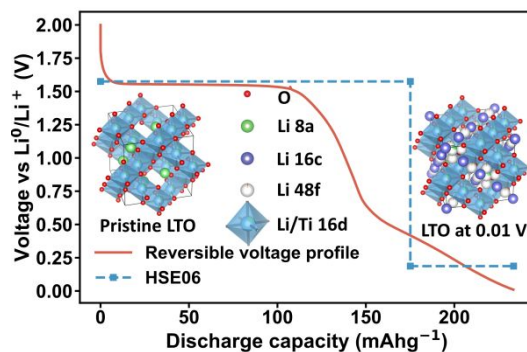
= These authors contributed equally to this work

Email: piliu@eng.ucsd.edu; ongsp@eng.ucsd.edu; huolinx@uci.edu

ABSTRACT

In this work, we show that the well-known lithium-ion anode material, $\text{Li}_4\text{Ti}_5\text{O}_{12}$, exhibits exceptionally high initial capacity of 310 mAh g^{-1} when it is discharged to 0.01 V . It maintains a reversible capacity of 230 mAh g^{-1} , far exceeding the “theoretical” capacity of 175 mAh g^{-1} when this anode is lithiated to the composition $\text{Li}_7\text{Ti}_5\text{O}_{12}$. Neutron diffraction analyses identify that additional Li reversibly inserts into the $\text{Li}_7\text{Ti}_5\text{O}_{12}$ to form $\text{Li}_8\text{Ti}_5\text{O}_{12}$. DFT calculations reveal the average potentials of the $\text{Li}_4\text{Ti}_5\text{O}_{12}$ to $\text{Li}_7\text{Ti}_5\text{O}_{12}$ step and the $\text{Li}_7\text{Ti}_5\text{O}_{12}$ to $\text{Li}_8\text{Ti}_5\text{O}_{12}$ step are 1.57 V and 0.19 V , respectively, which are in excellent agreement with experimental results. TEM studies confirm that the irreversible capacity of $\text{Li}_4\text{Ti}_5\text{O}_{12}$ during its first cycle originates from the formation of a solid electrolyte interface (SEI) layer. This work clarifies the fundamental lithiation mechanism of the $\text{Li}_4\text{Ti}_5\text{O}_{12}$, when lithiated to 0.01 V vs Li.

TOC Graphic for manuscript



1
2
3
4
5
6 $\text{Li}_4\text{Ti}_5\text{O}_{12}$ (LTO) is a well-known anode material for long-life, high rate Li-ion batteries. Its high
7
8 stability, excellent safety, and outstanding rate capability have led to its successful
9
10 commercialization.¹⁻⁷ LTO, or $[\text{Li}_3]^{8a}[\text{Li}_1\text{Ti}_5]^{16d}[\square]^{16c}[\text{O}_{12}]^{32e}$ possesses a spinel structure with Fd
11
12 $\bar{3}m$ space group. The lithiation mechanism is widely accepted that it takes 3 Li^+ per formula unit
13
14 to form $[\square]^{8a}[\text{Li}_1\text{Ti}_5]^{16d}[\text{Li}_6]^{16c}[\text{O}_{12}]^{32e}$.⁸ Accordingly, the theoretical capacity of LTO is
15
16 calculated to be 175 mAh g^{-1} . Its operating potential is at around 1.5 V vs Li/Li⁺. However, the
17
18 process of Li^+ intercalation into the $\text{Li}_4\text{Ti}_5\text{O}_{12}$ to form $\text{Li}_7\text{Ti}_5\text{O}_{12}$ only reduces 60% of the Ti^{4+} in
19
20 the crystal to the Ti^{3+} . If assuming fully utilization of the $\text{Ti}^{3+}/\text{Ti}^{4+}$ redox, the $\text{Li}_7\text{Ti}_5\text{O}_{12}$ is able to
21
22 take additional 2 Li^+ to form $\text{Li}_9\text{Ti}_5\text{O}_{12}$. As well agreed in a structural point of view, there are
23
24 additional vacancies to host up to 3 extra Li^+ at the 8a sites per unit cell to form $\text{Li}_9\text{Ti}_5\text{O}_{12}$ or
25
26 even $\text{Li}_{10}\text{Ti}_5\text{O}_{12}$. In principle, LTO has the capability to host more than 3 Li^+ per formula, which
27
28 will highly boost the capacity in LTO anode.
29
30
31
32
33

34
35 Since the $\text{Li}_7\text{Ti}_5\text{O}_{12}$ was treated as the discharge product of the LTO, earlier reported works
36
37 usually discharged the LTO to 1V.⁹ There have been several reports of cycling LTO to lower
38
39 potentials. Yi cycled the LTO between 0.01 V and 2.5 V and reported a first-cycle discharge
40
41 capacity of 270 mAh g^{-1} with a reversible capacity of 210 mAh g^{-1} .¹⁰⁻¹² Wang employed atomic-
42
43 resolution annular bright-field imaging and electron energy-loss spectroscopy to measure local
44
45 Li occupancy of LTO at 0.01 V. They observed partial re-occupation of 8a sites by further
46
47 lithiation of $\text{Li}_7\text{Ti}_5\text{O}_{12}$, and claimed that the increased capacity in LTO is due to the extra storage
48
49 of Li in the near-surface region.¹³ However, the microscopy based study mainly represent the
50
51 general lithiation mechanism in the localized surface of LTO. Ge investigated the structural
52
53 evolution of LTO between 0.01 V and 2.5 V via *in-situ* X-ray diffraction.¹⁴ Because of the low
54
55
56
57
58
59
60

1
2
3 scattering power of Li, their XRD refinement results qualitatively indicated the 8a sites of LTO
4 could host the extra Li in the bulk. Despite of these investigations, two outstanding questions
5 regarding the (de)lithiation mechanism of LTO still have not been resolved yet: (1) How much
6 Li^+ could reversibly insert into LTO and how are the Li^+ distributed at different sites? (2) What
7 causes the first cycle irreversible capacity of LTO discharged to 0.01 V?
8
9

10
11
12 In this work, we discharged and charged the LTO between 0.01 V and 2.0 V at first. The LTO
13 delivered an initial discharge capacity of 310 mAh g^{-1} , and showed a reversible capacity of 230
14 mAh g^{-1} . Taking advantage of the high sensitivity of neutron scattering to light elements such as
15 Li,¹⁵⁻¹⁶ we performed Rietveld analysis of neutron powder diffraction data to arrive at a reliable
16 and detailed crystal structural characterization of LTO.¹⁷⁻²⁰ The Li occupancies at different sites
17 were quantitatively identified. Our DFT calculations not only confirmed the structures of the
18 (de)lithiated LTO, but also explained the voltage profile of the LTO. Finally, an SEI layer with a
19 thickness of 12 nm was observed on the surface of the fully discharged LTO, which indicated
20 that the irreversible capacity in the first cycle was associated with the formation of the SEI.
21
22
23
24
25
26
27
28
29
30
31
32
33
34
35

36
37 Figure 1 compares the electrochemical performance of the LTO cycled with different voltage
38 windows. Both cells were cycled at a moderate current density of 20 mA g^{-1} . The cell cycled
39 with a cut-off voltage at 1.0 V exhibited an initial discharge capacity of 174 mAh g^{-1} , its capacity
40 was stabilized at 162 mAh g^{-1} after 10 cycles. This performance was consistent with previous
41 reports and corresponded to the process from $\text{Li}_4\text{Ti}_5\text{O}_{12}$ to $\text{Li}_7\text{Ti}_5\text{O}_{12}$.²¹ While the cell discharged
42 to 0.01 V delivered an exceptionally high capacity of 310 mAh g^{-1} for its first discharge, its
43 reversible capacity at 10th cycle was 233 mAh g^{-1} . The LTO displayed excellent cycling stability
44 for both cut-off voltages, indicating the process for the extra lithiation beyond $\text{Li}_7\text{Ti}_5\text{O}_{12}$ is highly
45 reversible. The voltage profiles present three characteristic regions during the first discharge. The
46
47
48
49
50
51
52
53
54
55
56
57
58
59
60

long plateau at 1.55 V is associated with the formation of the $\text{Li}_7\text{Ti}_5\text{O}_{12}$. Below 1.0 V, a bump at ~ 0.8 V and a slope under 0.6 V are observed. The bump disappeared after the first discharge, suggesting this electrochemical process is irreversible.

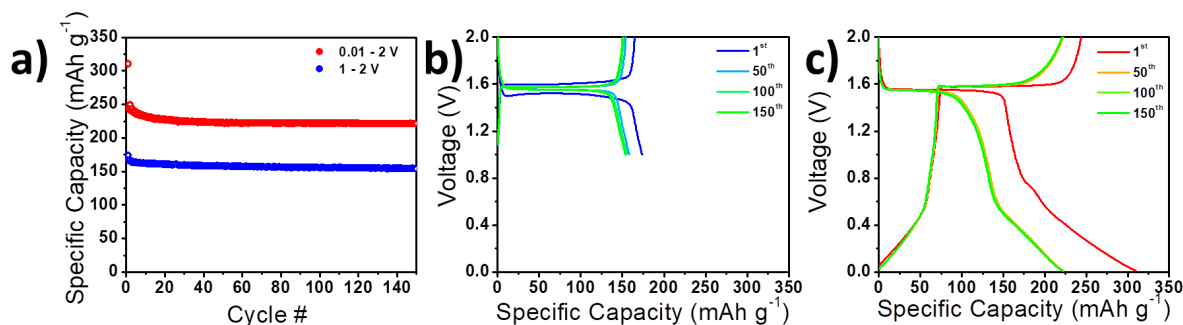


Figure 1. The comparison of electrochemical performance of LTO discharged to different voltages. a) capacities, b), and c) voltage profiles over the course of 150 cycles at 20 mA g^{-1} .

According to the capacity, the LTO takes in 5.3 Li during the first discharge, while only 4 Li reversibly participates in the following cycles. The irreversible Li may either be trapped into the LTO host, or be consumed by side reactions. A quantitative analysis of the Li site occupancies in the bulk of LTO at different states of (dis)charge will provide a direct understanding of the extra Li insertion mechanism of the LTO. Neutron diffraction was performed, due to its high sensitivity to Li, on LTO at a series of lithiation states.¹⁷⁻¹⁸ Figure 2a depicts the Rietveld refinement of the neutron diffraction profile of the pristine LTO. Its structure is well modeled by the spinel phase ($\text{Fd}\bar{3}\text{m}$).⁸ Figure 2b shows the structure of pristine LTO, the 32e sites are fully occupied by O atoms, the 16d sites are shared by Ti and Li at the ratio of 5:1, and the rest of Li fills the 8a sites (noted as $[\text{Li}_3]^{8\text{a}}[\text{Li}_1\text{Ti}_5]^{16\text{d}}[\text{O}_{12}]^{32\text{e}}$). Figure 2c summarizes the site occupancies of the Li in the LTO at different states of (dis)charge. The refined profiles and detailed structure information are presented in the Supporting Information (Figure S1-5, Table S1-5). During the long plateau region on discharge, 3 Li insert into LTO at 16c sites accompanied by a large amount of the Li transferring from the 8a sites to the 16c sites to form

1
2
3 [Li_{0.16}]^{8a}[Li₁Ti₅]^{16d}[Li_{5.84}]^{16c}[O₁₂]^{32e}. Further discharge of LTO to 0.01 V only takes 1 Li, which
4 fills the 16c sites first, then distributes between the 8a sites and the 48f sites. The LTO at 0.01 V
5
6 can be described as [Li_{0.62}]^{8a}[Li₁Ti₅]^{16d}[Li₆]^{16c}[Li_{0.38}]^{48f}[O₁₂]^{32e}. Once charged back to 1.0 V, the
7
8 LTO structure turns into the [Li_{0.16}]^{8a}[Li₁Ti₅]^{16d}[Li_{5.84}]^{16c}[O₁₂]^{32e} again. After one electrochemical
9
10 cycle, the LTO structure is noted as [Li_{2.57}]^{8a}[Li₁Ti₅]^{16d}[Li_{0.43}]^{16c}[O₁₂]^{32e}, suggesting the Li is
11
12 extracted from the 16c sites, while a certain amount of Li transfers back to the 8a sites.
13
14 Significantly, there is Li located at 16c sites in the delithiated LTO, which differs from the
15
16 pristine LTO. The neutron diffraction refinements identify that 4 Li are reversibly intercalated
17
18 into the LTO.
19
20
21
22
23

24 Besides the Li occupancies, the crystal lattice changes of LTO are studied as well.¹⁹⁻²⁰ Figure 2d
25 shows that despite 4 Li entering the crystal, the lattice change of the LTO is very small. The
26
27 volume of the Li₇Ti₅O₁₂ unit cell is only 0.18% smaller than the Li₄Ti₅O₁₂, leading to its
28
29 reputation as a “zero-strain” material.^{3, 22} The Li₈Ti₅O₁₂ shows a 1.08% volume expansion as
30
31 compared to the Li₄Ti₅O₁₂, still extremely minor. Figure 2e exhibits the evolution of the Ti-O
32
33 bond length. At the pristine state, the Ti-O bond is 1.9892 Å. As 3 Li insert into the LTO, the Ti-
34
35 O bond increases to 2.0302 Å in Li₇Ti₅O₁₂. The Li₈Ti₅O₁₂ shows the longest Ti-O bond of
36
37 2.0434 Å. The increase of the Ti-O bond indicates the reduction of the Ti caused by the Li
38
39 insertion. During charging, the Ti-O bond length decreases. The Ti-O bond of Li₄Ti₅O₁₂ after
40
41 one cycle becomes 1.9958 Å, which is slightly larger than the pristine LTO. This difference may
42
43 come from the change in Li occupancies at 8a and 16c sites.
44
45
46
47
48
49
50
51
52
53
54
55
56
57
58
59
60

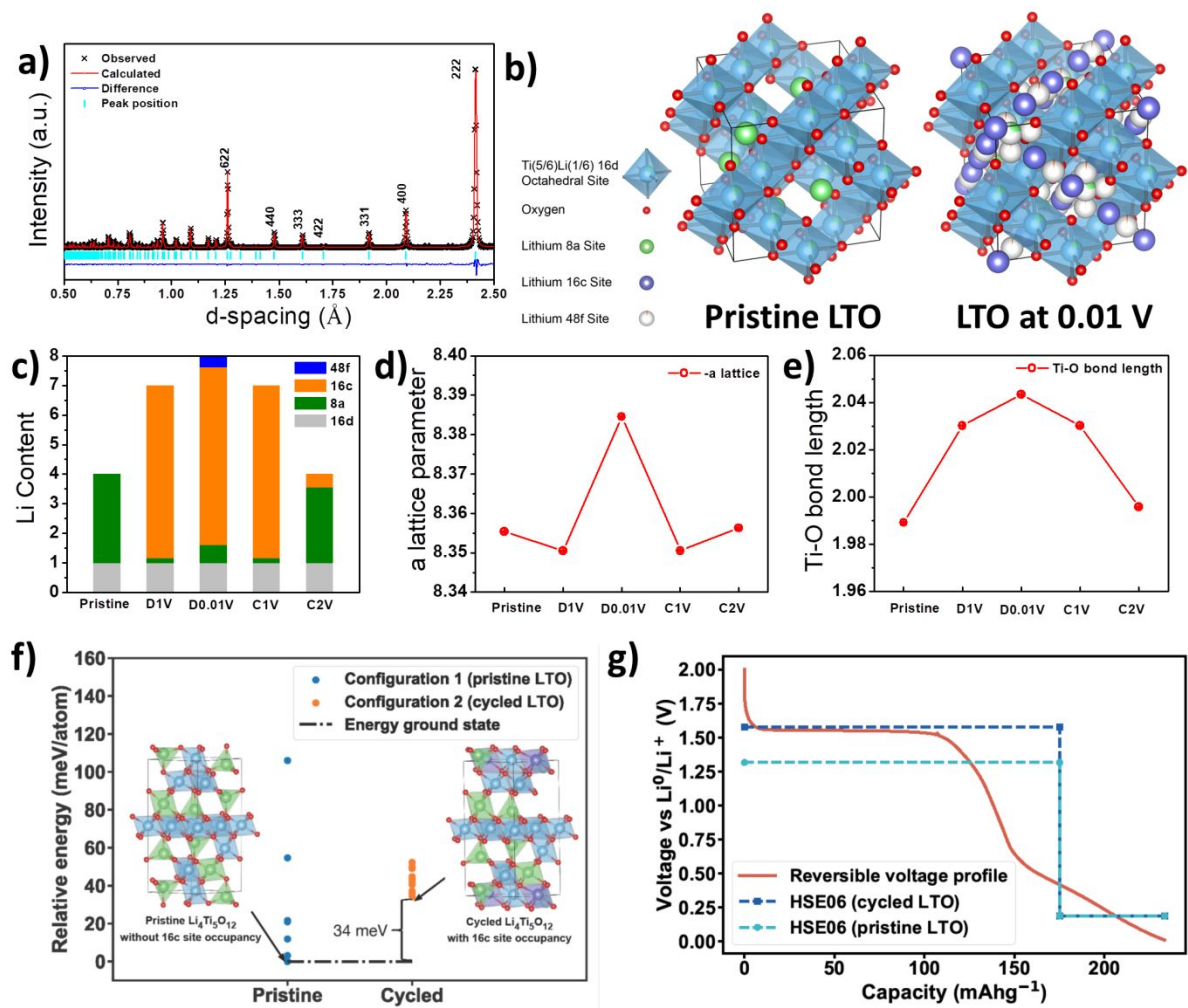


Figure 2. The crystal structure analysis of LTO at different states of (dis)charge via neutron diffraction. a) neutron diffraction refinement of pristine LTO, b) crystal structure of pristine LTO and LTO at 0.01 V on first discharge, c) Li site occupancies at different states of (dis)charge, d) lattice parameters, e) Ti-O bond lengths. f) relative energy for different orderings of pristine and cycled $\text{Li}_4\text{Ti}_5\text{O}_{12}$, g) voltage profiles of simulated curves using HSE06 functional (with pristine/cycled state of $\text{Li}_4\text{Ti}_5\text{O}_{12}$) and reversible experimental capacity after stable SEI formation.

We performed DFT calculations using GGA functional²³ on all symmetrically distinct orderings of pristine ($[\text{Li}_3]^{8a}[\text{Li}_1\text{Ti}_5]^{16d}[\text{O}_{12}]^{32e}$) and cycled $\text{Li}_4\text{Ti}_5\text{O}_{12}$ ($[\text{Li}_{2.5}]^{8a}[\text{Li}_1\text{Ti}_5]^{16d}[\text{Li}_{0.5}]^{16c}[\text{O}_{12}]^{32e}$). As shown in Figure 2f, we find that the lowest energy ordering of the cycled material is only 34 meV higher than the lowest energy ordering of the pristine material. This suggests that the

1
2
3 metastable state with a small 16c site occupancy is accessible through electrochemical cycling at
4
5 room temperature.²⁴
6

7
8 Figure 2g shows the voltage profile of for up to 4 Li insertion into LTO with stable phases at $x=4$,
9
10 7, 8 in $\text{Li}_x\text{Ti}_5\text{O}_{12}$ computed using the HSE06 functional.²⁵⁻²⁶ The average voltage for 3 Li
11
12 insertion computed using HSE06 functional (1.57 V vs Li/Li⁺) is in excellent agreement with
13
14 well-known experimental LTO voltage between $\text{Li}_4\text{Ti}_5\text{O}_{12}$ and $\text{Li}_7\text{Ti}_5\text{O}_{12}$ (1.55 V vs Li/Li⁺).²⁷⁻²⁸
15
16 We note that the voltage profile computed using the metastable cycled $\text{Li}_4\text{Ti}_5\text{O}_{12}$ is in much
17
18 better agreement compared to that computed using the pristine $\text{Li}_4\text{Ti}_5\text{O}_{12}$, further supporting the
19
20 results of the LTO neutron diffraction. When discharging to a very low voltage of 0.01 V, an
21
22 additional Li can be intercalated into LTO with reversible capacity up to 233 mAh g⁻¹. The
23
24 computed voltage for this additional Li insertion from $\text{Li}_7\text{Ti}_5\text{O}_{12}$ to $\text{Li}_8\text{Ti}_5\text{O}_{12}$ is 0.19 V, which is
25
26 again in excellent agreement with the 0.21 V that is obtained from reversible voltage profile after
27
28 stable SEI formation.
29
30
31
32
33

34
35 In order to investigate the charge compensation mechanism during Li-ion insertion and
36
37 extraction, X-ray absorption spectroscopy (XAS) measurements were conducted with Ti K-edge
38
39 at different states of (dis)charge. Normalized Ti K-edge X-ray absorption near edge structure
40
41 (XANES) spectra are shown in Figure 3a. There are three characteristic regions in the spectra,
42
43 the pre-edge peaks at ~4969 eV, shoulder peaks at ~4975 eV, and peaks at ~4986 eV. It is
44
45 evident that the pristine $\text{Li}_4\text{Ti}_5\text{O}_{12}$ compound predominantly consists of Ti⁴⁺.²⁹ Clear changes are
46
47 shown in the Ti XANES spectra upon the discharge and charge process. The Ti K-edge pre-edge
48
49 intensity is reduced after the lithiation plateau, suggesting the oxidation state of Ti at 1.0 V is
50
51 lower than Ti⁴⁺.³⁰ An evident shift of the absorption energy to the lower energy region is
52
53 observed in the LTO at 0.01 V compared to that of the pristine state. The amount of absorption
54
55
56
57
58
59
60

energy shift is ~ 2 eV, suggesting that the oxidation state of Ti is further reduced. After first charge, the oxidation state of Ti returns back to tetravalent. Based on the Ti XANES, it is proved that Ti is the only electrochemically active species. We can also demonstrate Ti reduction (from Ti^{4+} to Ti^{3+}) in the lithiation process through the averaged integrated spin density for Ti from our DFT calculations³¹ in Figure 3b. Ti^{4+} , which has the $3d^04s^0$ electron configuration, has a net spin of 0, while Ti^{3+} has a net spin of 1. For $\text{Li}_4\text{Ti}_5\text{O}_{12}$, all Ti are in the 4+ oxidation state, and hence, the average integrated spin density is 0. When 3 Li are inserted to form $\text{Li}_7\text{Ti}_5\text{O}_{12}$, 3 Ti are reduced to 3+, resulting in an average integrated spin density of approximately $3/5 = 0.6 \mu_B$ at a radius of 2.0 angstroms from Ti. When a further Li is inserted to form $\text{Li}_8\text{Ti}_5\text{O}_{12}$, 4 Ti are in the 3+ oxidation state, resulting in an average integrated spin density of $4/5 = 0.8 \mu_B$ at the same radius.

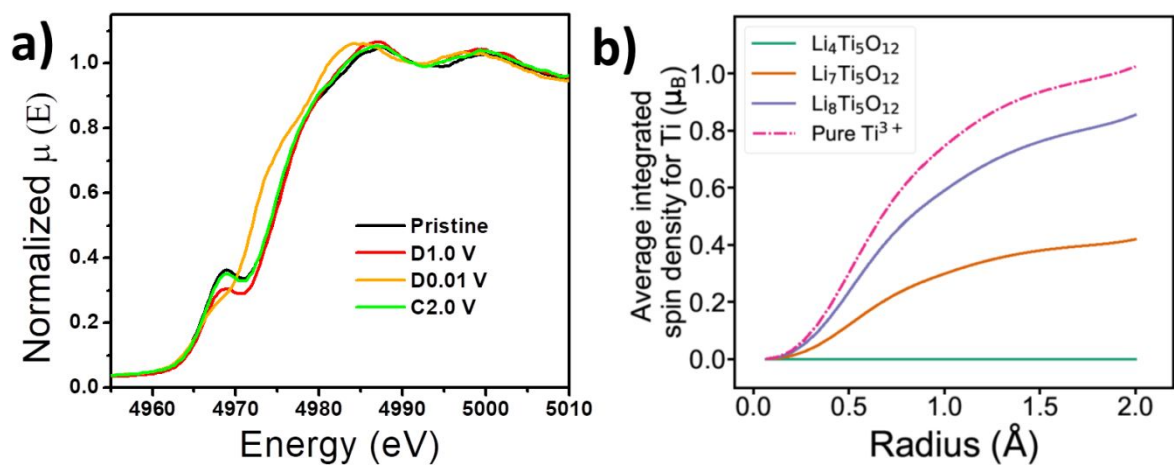


Figure 3. The charge compensation mechanism of LTO. a) The Ti K-edge at different states of (dis)charge, b) average integrated spin density for Ti as a function of radius from Ti up to 2\AA .

The neutron diffraction results show only 4 Li intercalate into the LTO during the first discharge, implying the irreversible capacity loss during the first cycle is associated with the side reactions between the electrode and electrolyte, especially at the surface of the electrode. High-resolution

transmission electron microscopy was used to examine the LTO discharged to different voltages. Figure 4a-b show the low magnification TEM images of the LTO at 1 V. The LTO particle is around 500 nm with a clean surface. In comparison, Figure 4c-d show that the LTO at 0.01 V is covered by an amorphous SEI layer with a thickness of 12 nm. Figure 4e is a statistical investigation of the SEI layers. The thickness of the SEI ranges from 9 - 17 nm. The formation of the SEI is irreversible, which is related to the bump at ~ 0.8 V in the first discharge profile. Consequently, the generation of SEI is responsible for the first cycle capacity loss. It is also possible that some electrolyte related side reactions take place on the conductive carbon. Figure 4f-g depicts the atomic resolution HAADF-STEM of $\text{Li}_8\text{Ti}_5\text{O}_{12}$. The presented images were measured from close to the [10-1] zone axis. The fast Fourier transform (FFT) result shows that the particle maintains a spinel structure, which is consistent with the neutron diffraction data.

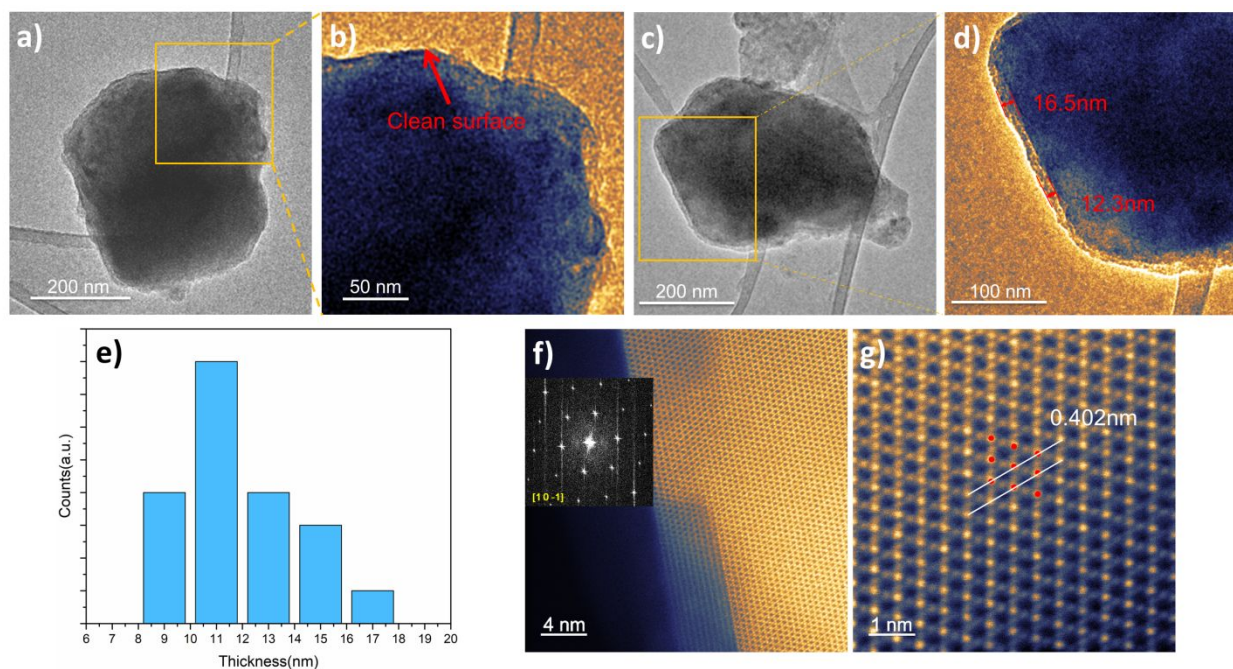
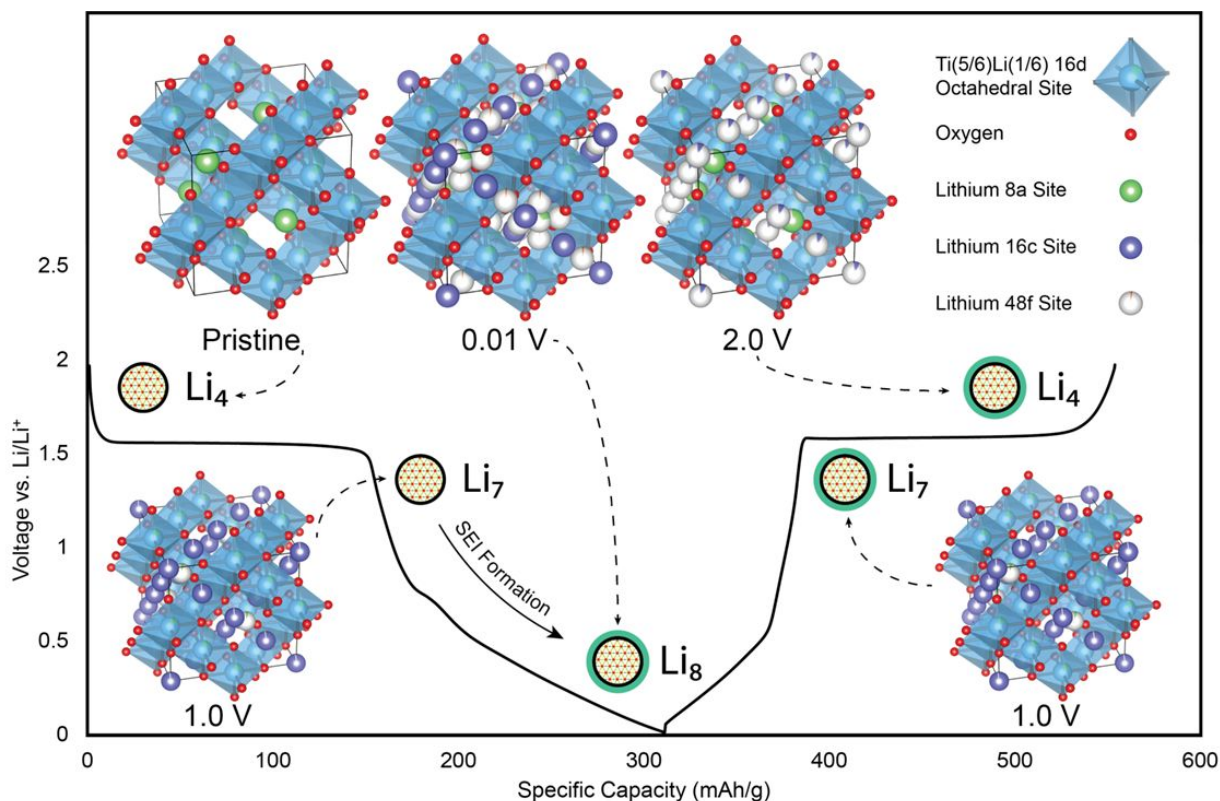


Figure 4. The morphological investigation on LTO at different states of discharge via microscopy. a), b) TEM images of LTO at 1 V on first discharge, c), d) TEM images of LTO at 0.01 V on first discharge, e) the statistic results of SEI thickness on the surface of LTO at 0.01 V on first discharge, f), g) atomic resolution HAADF-STEM from close to [10-1] zone axis of LTO at 0.01 V on first discharge.

1
2
3 Scheme 1 summarizes our understanding on the working mechanisms of the LTO. The structure
4 of the pristine LTO is $[\text{Li}_3]^{8a}[\text{Li}_1\text{Ti}_5]^{16d}[\text{O}_{12}]^{32e}$, which is consistent with the previous
5 literatures.³² After the 1.55 V plateau in the discharge, $\text{Li}_4\text{Ti}_5\text{O}_{12}$ transforms to
6 $[\text{Li}_{0.16}]^{8a}[\text{Li}_1\text{Ti}_5]^{16d}[\text{Li}_{5.84}]^{16c}[\text{O}_{12}]^{32e}$. Besides the 3 Li enter the 16c sites in LTO crystal, the Li
7 also move from the original 8a sites to the 16c sites. Continued discharging of LTO to 0.01 V not
8 only takes one extra Li into the LTO bulk, but also promotes electrolyte reduction at the LTO
9 surface to form a thick SEI layer. The fully discharged LTO is noted as
10 $[\text{Li}_{0.62}]^{8a}[\text{Li}_1\text{Ti}_5]^{16d}[\text{Li}_6]^{16c}[\text{Li}_{0.38}]^{48f}[\text{O}_{12}]^{32e}$, with 8a and 48f sites been partially occupied. Once
11 the LTO is charged back to 1.0 V, its structure recovers to exactly the same as it is discharged to
12 1.0 V. The fully delithiated LTO doesn't return to the pristine structure, with a fraction of Li
13 staying at the 16c sites ($[\text{Li}_{2.57}]^{8a}[\text{Li}_1\text{Ti}_5]^{16d}[\text{Li}_{0.43}]^{16c}[\text{O}_{12}]^{32e}$). The volume change of the LTO
14 unit cell is small during the whole process, and the transformation between $\text{Li}_4\text{Ti}_5\text{O}_{12}$ and
15 $\text{Li}_8\text{Ti}_5\text{O}_{12}$ is highly reversible, which leads to its excellent cycling stability. The charge transfer
16 during the Li (de)intercalation is compensated by the $\text{Ti}^{3+}/\text{Ti}^{4+}$ redox.
17
18
19
20
21
22
23
24
25
26
27
28
29
30
31
32
33
34
35
36
37
38
39
40
41
42
43
44
45
46
47
48
49
50
51
52
53
54
55
56
57
58
59
60



Scheme 1. Schematic of the energy storage mechanism of the LTO.

By using a combination of electrochemical and structural characterization methods, we have identified the charge storage mechanism in LTO, particularly when cycled to 0.01 V. Quantitative analysis of neutron diffraction data identified the limit of Li insertion into the LTO spinel to be 4, with very minor change in lattice parameters which led to highly reversible electrochemical performance. The robustness of the host structure is confirmed by TEM studies. Ti is the sole redox species involved in the charge storage reactions as confirmed by XANES studies and average integrated spin from simulations. We used DFT calculations to confirm the feasibility of structural difference between pristine and cycled LTO and the voltage profile calculated by HSE06 functional is very close to experimental one. The irreversible capacity loss in its first cycle is caused by the thick SEI formation. The statistic TEM studies show an amorphous SEI layer with thickness of around 12nm. Our work clearly established that

1
2
3 reversible intercalation reactions in oxides are possible at potentials close to Li. The insight may
4
5 be used to design and optimize other intercalation type anode materials.
6
7
8
9
10
11
12
13
14
15
16
17
18
19
20
21
22
23
24
25
26
27
28
29
30
31
32
33
34
35
36
37
38
39
40
41
42
43
44
45
46
47
48
49
50
51
52
53
54
55
56
57
58
59
60

1
2
3 This manuscript has been authored by UT-Battelle, LLC under Contract No. DE-AC05-
4 00OR22725 with the U.S. Department of Energy. The United States Government retains and the
5
6 publisher, by accepting the article for publication, acknowledges that the United States
7
8 Government retains a non-exclusive, paid-up, irrevocable, worldwide license to publish or
9
10 reproduce the published form of this manuscript, or allow others to do so, for United States
11
12 Government purposes. The Department of Energy will provide public access to these results of
13
14 federally sponsored research in accordance with the DOE Public Access Plan
15
16 (<http://energy.gov/downloads/doe-public-access-plan>).
17
18
19
20
21
22
23
24
25
26
27
28
29
30
31
32
33
34
35
36
37
38
39
40
41
42
43
44
45
46
47
48
49
50
51
52
53
54
55
56
57
58
59
60

Acknowledgement

This work was supported by the Office of Vehicle Technologies of the U.S. Department of Energy through the Advanced Battery Materials Research (BMR) Program (Battery500 Consortium) under Contract DE-EE0007764. Part of the work used the UCSD-MTI Battery Fabrication Facility and the UCSD-Arbin Battery Testing Facility. Z.Z., X.L. and S.P.O. acknowledge funding from the U.S. Department of Energy, Office of Science, Basic Energy Sciences under Award No. DE-SC0012118 for the computational part of this work as well as computing resources provided by Triton Shared Computing Cluster (TSCC) at the UC San Diego, the National Energy Research Scientific Computing Center (NERSC), and the Extreme Science and Engineering Discovery Environment (XSEDE) supported by the National Science Foundation under Grant ACI-1053575. Neutron diffraction work was carried out at the Spallation Neutron Source (SNS), which is the U.S. Department of Energy (DOE) user facility at the Oak Ridge National Laboratory, sponsored by the Scientific User Facilities Division, Office of Basic Energy Sciences. Work done by R.Z. and H.X. is in part supported by the U.S. Department of Energy's Office of Energy Efficiency and Renewable Energy (EERE) under the Award Number: DE-EE0008444. R.L. is supported by the Assistant Secretary for Energy Efficiency and Renewable Energy, Vehicle Technology Office of the U.S. Department of Energy through the Advanced Battery Materials Research (BMR) Program, including Battery500 Consortium under contract DE-SC0012704. This research used resources of the Center for Functional Nanomaterials, which is a U.S. DOE Office of Science Facility, at Brookhaven National Laboratory under Contract No. DE-SC0012704.

Supporting Information

1
2
3 The Supporting Information is available free of charge on the ACS Publications website at DOI:
4
5 XXXXXX.
6
7

8 Experimental methods (synthesis of LTO, electrochemical tests, neutron diffraction, XAS
9 spectra and STEM); DFT calculations; neutron diffraction and refined data of LTO.
10
11
12
13
14
15
16
17
18
19
20
21
22
23
24
25
26
27
28
29
30
31
32
33
34
35
36
37
38
39
40
41
42
43
44
45
46
47
48
49
50
51
52
53
54
55
56
57
58
59
60

1. Yuan, T.; Tan, Z. P.; Ma, C. R.; Yang, J. H.; Ma, Z. F.; Zheng, S. Y., Challenges of Spinel $\text{Li}_4\text{Ti}_5\text{O}_{12}$ for Lithium-Ion Battery Industrial Applications. *Adv. Energy Mater.* **2017**, *7*, 1601625.
2. Hao, X. G.; Bartlett, B. M., $\text{Li}_4\text{Ti}_5\text{O}_{12}$ Nanocrystals Synthesized by Carbon Templating from Solution Precursors Yield High Performance Thin Film Li-Ion Battery Electrodes. *Adv. Energy Mater.* **2013**, *3*, 753-761.
3. Ohzuku, T.; Ueda, A.; Yamamoto, N., Zero-Strain Insertion Material of $\text{Li}[\text{Li}_{1/3}\text{Ti}_{5/3}]\text{O}_4$ for Rechargeable Lithium Cells. *J. Electrochem. Soc.* **1995**, *142*, 1431-1435.
4. Aravindan, V.; Lee, Y. S.; Madhavi, S., Research Progress on Negative Electrodes for Practical Li-Ion Batteries: Beyond Carbonaceous Anodes. *Adv. Energy Mater.* **2015**, *5*, 1402225.
5. Zhao, B. T.; Deng, X.; Ran, R.; Liu, M. L.; Shao, Z. P., Facile Synthesis of a 3D Nanoarchitected $\text{Li}_4\text{Ti}_5\text{O}_{12}$ Electrode for Ultrafast Energy Storage. *Adv. Energy Mater.* **2016**, *6*, 1500924.
6. Han, X.; Gui, X.; Yi, T. F.; Li, Y. W.; Yue, C. B., Recent progress of NiCo_2O_4 -based anodes for high-performance lithium-ion batteries. *Curr. Opin. Solid St. M.* **2018**, *22*, 109-126.
7. Yi, T. F.; Zhu, Y. R.; Tao, W.; Luo, S.; Xie, Y.; Li, X. F., Recent advances in the research of $\text{MLi}_2\text{Ti}_6\text{O}_{14}$ ($M=2\text{Na, Sr, Ba, Pb}$) anode materials for Li-ion batteries. *J. Power Sources* **2018**, *399*, 26-41.
8. Pang, W. K.; Peterson, V. K.; Sharma, N.; Shiu, J. J.; Wu, S. H., Lithium Migration in $\text{Li}_4\text{Ti}_5\text{O}_{12}$ Studied Using in Situ Neutron Powder Diffraction. *Chem. Mater.* **2014**, *26*, 2318-2326.
9. Odziomek, M.; Chaput, F.; Rutkowska, A.; Swierczek, K.; Olszewska, D.; Sitarz, M.; Lerouge, F.; Parola, S., Hierarchically structured lithium titanate for ultrafast charging in long-life high capacity batteries. *Nat. Commun.* **2017**, *8*, 1-7.
10. Yi, T. F.; Yang, S. Y.; Xie, Y., Recent advances of $\text{Li}_4\text{Ti}_5\text{O}_{12}$ as a promising next generation anode material for high power lithium-ion batteries. *J. Mater. Chem. A* **2015**, *3*, 5750-5777.
11. Yi, T. F.; Xie, Y.; Zhu, Y. R.; Zhu, R. S.; Shen, H. Y., Structural and thermodynamic stability of $\text{Li}_4\text{Ti}_5\text{O}_{12}$ anode material for lithium-ion battery. *J. Power Sources* **2013**, *222*, 448-454.
12. Yi, T. F.; Xie, Y.; Wu, Q. J.; Liu, H. P.; Jiang, L. J.; Ye, M. F.; Zhu, R. S., High rate cycling performance of lanthanum-modified $\text{Li}_4\text{Ti}_5\text{O}_{12}$ anode materials for lithium-ion batteries. *J. Power Sources* **2012**, *214*, 220-226.
13. Wang, F.; Wu, L. J.; Ma, C.; Su, D.; Zhu, Y. M.; Graetz, J., Excess lithium storage and charge compensation in nanoscale $\text{Li}_{4+x}\text{Ti}_5\text{O}_{12}$. *Nanotechnology* **2013**, *24*, 424006.
14. Ge, H.; Li, N.; Li, D. Y.; Dai, C. S.; Wang, D. L., Study on the Theoretical Capacity of Spinel Lithium Titanate Induced by Low-Potential Intercalation. *J. Phys. Chem. C* **2009**, *113*, 6324-6326.
15. Chen, Y.; Rangasamy, E.; Lang, C. D.; An, K., Origin of High Li^+ Conduction in Doped $\text{Li}_7\text{La}_3\text{Zr}_2\text{O}_{12}$ Garnets. *Chem. Mater.* **2015**, *27*, 5491-5494.
16. Liu, X.; Chen, Y.; Hood, Z. D.; Ma, C.; Yu, S.; Sharafi, A.; Wang, H.; An, K.; Sakamoto, J.; Siegel, D. J.; Cheng, Y.; Jalarvo, N. H.; Chi, M., Elucidating the mobility of H^+ and Li^+ ions in $(\text{Li}_{6.25-x}\text{H}_x\text{Al}_{0.25})\text{La}_3\text{Zr}_2\text{O}_{12}$ via correlative neutron and electron spectroscopy. *Energ. Environ. Sci.* **2019**, *12*, 945-951.
17. Liu, H. D.; Liu, H.; Seymour, I. D.; Chernova, N.; Wiaderek, K. M.; Trease, N. M.; Hy, S.; Chen, Y.; An, K.; Zhang, M. H.; Borkiewicz, O. J.; Lapidus, S. H.; Qiu, B.; Xia, Y. G.; Liu, Z. P.; Chupas, P. J.; Chapman, K. W.; Whittingham, M. S.; Grey, C. P.; Meng, Y. S., Identifying the chemical and structural irreversibility in $\text{LiNi}_{0.8}\text{Co}_{0.15}\text{Al}_{0.05}\text{O}_2$ - a model compound for classical layered intercalation. *J. Mater. Chem. A* **2018**, *6*, 4189-4198.
18. Liu, H.; Liu, H. D.; Lapidus, S. H.; Meng, Y. S.; Chupas, P. J.; Chapman, K. W., Sensitivity and Limitations of Structures from X-ray and Neutron-Based Diffraction Analyses of Transition Metal Oxide Lithium-Battery Electrodes. *J. Electrochem. Soc.* **2017**, *164*, A1802-A1811.
19. Liu, H. D.; Chen, Y.; Hy, S.; An, K.; Venkatachalam, S.; Qian, D. N.; Zhang, M. H.; Meng, Y. S., Operando Lithium Dynamics in the Li-Rich Layered Oxide Cathode Material via Neutron Diffraction. *Adv. Energy Mater.* **2016**, *6*, 1502143.

- 1
2
3 20. Liu, H. D.; Fell, C. R.; An, K.; Cai, L.; Meng, Y. S., In-situ neutron diffraction study of the
4 $x\text{Li}_{(2)}\text{MnO}_{(3)}\text{center dot}(1-x)\text{LiMO}_2$ ($x=0, 0.5$; $M = \text{Ni, Mn, Co}$) layered oxide compounds during
5 electrochemical cycling. *J. Power Sources* **2013**, *240*, 772-778.
- 6 21. Zhang, Q. Y.; Verde, M. G.; Seo, J. K.; Li, X.; Meng, Y. S., Structural and electrochemical properties
7 of Gd-doped $\text{Li}_4\text{Ti}_5\text{O}_{12}$ as anode material with improved rate capability for lithium-ion batteries. *J*
8 *Power Sources* **2015**, *280*, 355-362.
- 9 22. Ariyoshi, K.; Yamamoto, S.; Ohzuku, T., Three-volt lithium-ion battery with $\text{Li}[\text{Ni}_{1/2}\text{Mn}_{3/2}]\text{O}_4$ and
10 the zero-strain insertion material of $\text{Li}[\text{Li}_{1/3}\text{Ti}_{5/3}]\text{O}_4$. *J. Power Sources* **2003**, *119*, 959-963.
- 11 23. Perdew, J. P.; Burke, K.; Ernzerhof, M., Generalized gradient approximation made simple. *Phys.*
12 *Rev. Lett.* **1996**, *77*, 3865-3868.
- 13 24. Zhu, Z. Y.; Chu, I. H.; Ong, S. P., $\text{Li}_3\text{Y}(\text{PS}_4)_{(2)}$ and $\text{Li}_5\text{PS}_4\text{Cl}_2$: New Lithium Superionic Conductors
14 Predicted from Silver Thiophosphates using Efficiently Tiered Ab Initio Molecular Dynamics Simulations.
15 *Chem. Mater.* **2017**, *29*, 2474-2484.
- 16 25. Chevrier, V. L.; Ong, S. P.; Armiento, R.; Chan, M. K. Y.; Ceder, G., Hybrid density functional
17 calculations of redox potentials and formation energies of transition metal compounds. *Phys. Rev. B*
18 **2010**, *82*, 075122.
- 19 26. Heyd, J.; Scuseria, G. E.; Ernzerhof, M., Hybrid functionals based on a screened Coulomb
20 potential. *J. Chem. Phys.* **2003**, *118*, 8207-8215.
- 21 27. Chen, S.; Xin, Y. L.; Zhou, Y. Y.; Ma, Y. R.; Zhou, H. H.; Qi, L. M., Self-supported $\text{Li}_4\text{Ti}_5\text{O}_{12}$
22 nanosheet arrays for lithium ion batteries with excellent rate capability and ultralong cycle life. *Energ.*
23 *Environ. Sci.* **2014**, *7*, 1924-1930.
- 24 28. Shi, Y.; Tang, H. M.; Jiang, S. L.; Kayser, L. V.; Li, M. Q.; Liu, F.; Ji, F.; Lipomi, D. J.; Ong, S. P.; Chen,
25 Z., Understanding the Electrochemical Properties of Naphthalene Diimide: Implication for Stable and
26 High-Rate Lithium-Ion Battery Electrodes. *Chem. Mater.* **2018**, *30*, 3508-3517.
- 27 29. Kim, C.; Yu, Y. S.; Moyon, B.; Sirisopanaporn, C.; Richardson, T. J.; Cabana, J., Visualization of the
28 Phase Propagation within Carbon -Free $\text{Li}_4\text{Ti}_5\text{O}_{12}$ Battery Electrodes. *J. Phys. Chem. C* **2016**, *120*, 29030-
29 29038.
- 30 30. Zhang, W.; Topsakal, M.; Cama, C.; Pelliccione, C. J.; Zhao, H.; Ehrlich, S.; Wu, L. J.; Zhu, Y. M.;
31 Frenkel, A. I.; Takeuchi, K. J.; Takeuchi, E. S.; Marschilok, A. C.; Lu, D. Y.; Wang, F., Multi-Stage Structural
32 Transformations in Zero-Strain Lithium Titanate Unveiled by in Situ X-ray Absorption Fingerprints. *J. Am.*
33 *Chem. Soc.* **2017**, *139*, 16591-16603.
- 34 31. Feng, X. Y.; Chien, P. H.; Zhu, Z. Y.; Chu, I. H.; Wang, P. B.; Immediato-Scuotto, M.; Arabzadeh, H.;
35 Ong, S. P.; Hu, Y. Y., Studies of Functional Defects for Fast Na-Ion Conduction in $\text{Na}_{3-y}\text{PS}_{4-x}\text{Cl}_x$ with a
36 Combined Experimental and Computational Approach. *Adv. Funct. Mater.* **2019**, *29*, 1807951.
- 37 32. Verde, M. G.; Baggetto, L.; Balke, N.; Veith, G. M.; Seo, J. K.; Wang, Z. Y.; Meng, Y. S., Elucidating
38 the Phase Transformation of $\text{Li}_4\text{Ti}_5\text{O}_{12}$ Lithiation at the Nanoscale. *Acs Nano* **2016**, *10*, 4312-4321.
- 39
40
41
42
43
44
45
46
47
48
49
50
51
52
53
54
55
56
57
58
59
60